
Figures and figure supplements

Two different cell-cycle processes determine the timing of cell division in *Escherichia coli*

Alexandra Colin et al

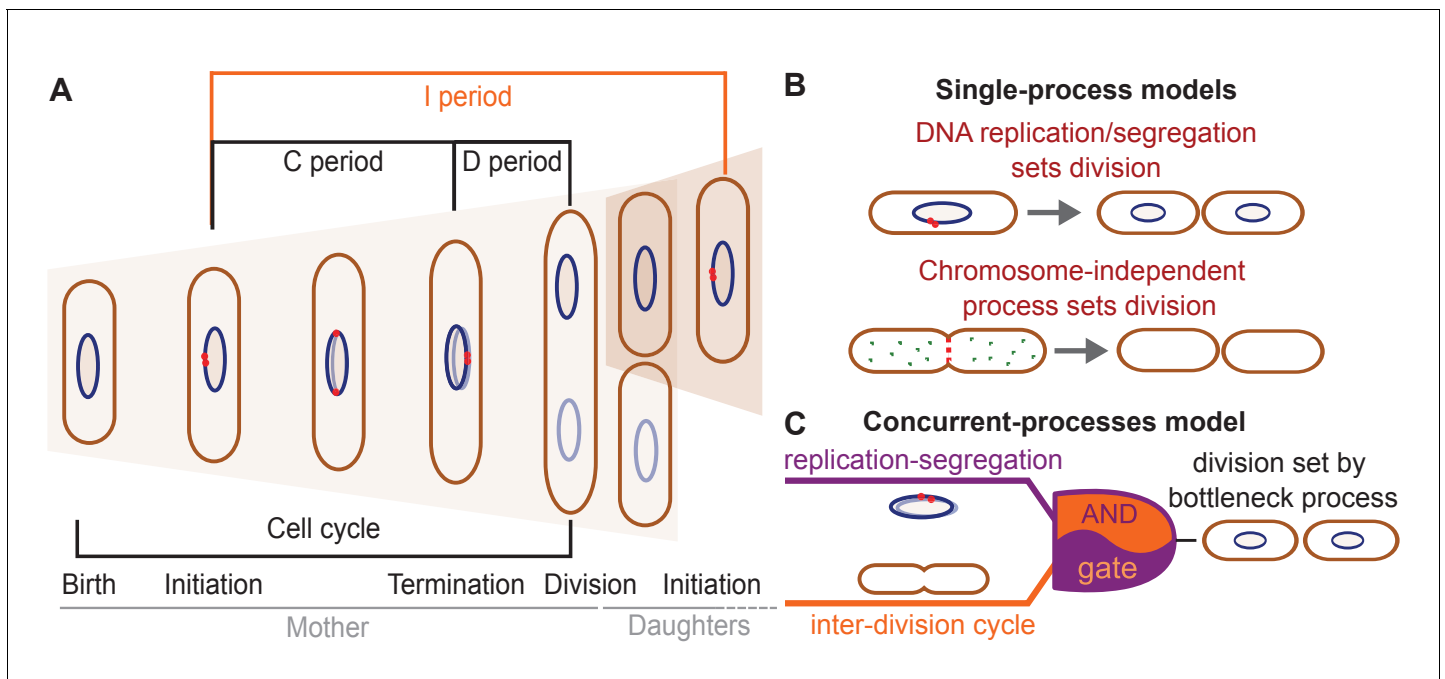


Figure 1. Different models have been suggested for cell-division control. **(A)** Cartoon of the cell cycle and definition of C, D and I periods. The C period is the time between initiation and termination of chromosome replication, the D period is the time between replication termination and division, and the I period is the time between subsequent initiations. **(B)** Models of cell-division control based on a single limiting process. According to the first set of models cell division is controlled by DNA replication and subsequent segregation (Witz et al., 2019; Ho and Amir, 2015; Sompayrac and Maaloe, 1973). According to the second set of models, cell division is controlled by a chromosome-independent inter-division process between birth and division (Si et al., 2017; Si et al., 2019; Harris and Theriot, 2016; Harris and Theriot, 2018). **(C)** Scheme of the concurrent-processes model. According to this model, the time of cell division is set by the slowest of two process, an inter-division process and chromosome replication/segregation. When both processes are completed, the cell can go through division (analogous to an AND gate).

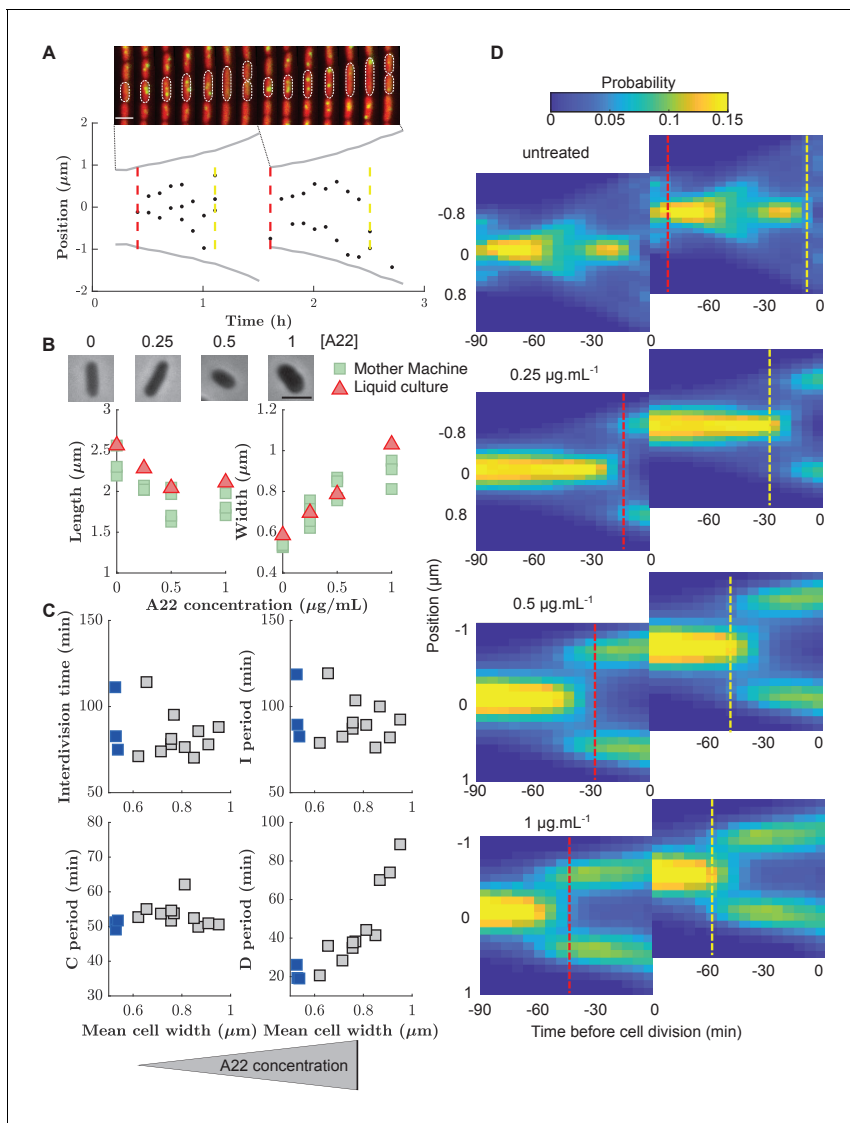


Figure 2. Increasing cell width through A22 increases the D period. (A) Top: Snapshots of a single mother-machine channel. Interval between images is 12 min. Red: cytoplasmic mCherry, yellow: YPet-DnaN. The contours show a cell growing for two consecutive cell cycles. Bottom: Cell length (gray line), the position of YPet-DnaN foci along the long axis of the cell (black dots), initiation and termination times (red and yellow dashed lines, respectively) in the same cells shown in A. Scale bar: 2 μm . (B) Top: Snapshots of *E. coli* S233 (NCM3722, λ ::*P-mcherry*, *dnaN*::*Ypet-dnaN*) treated with sublethal amounts of A22 (concentrations in $\mu\text{g.mL}^{-1}$). Scale bar: 2 μm . Bottom: Effect of A22 treatment on average dimensions of cells grown in liquid or in mother machine for at least 6 hr of exponential growth. For cell-to-cell variations see Figure (C). Duration of inter-division time, I, C, and D periods as a function of average cell width measured in mother machines. Blue and gray squares represent unperturbed conditions and A22-treatment, respectively. Each symbol represents an independent biological replicate. (D) Conditional probability density of the occurrence of YPet-DnaN foci $p(y|t)$ as a function of cell length (y-axis) for different time points before subsequent cell division (x-axis) for different A22 concentrations as indicated on top of the maps. Maps are duplicated for better visualization of the replication process. Vertical lines indicate the beginning and end of the probability peaks that correspond to replication initiation and termination, respectively. Note that these times do not strictly agree with average replication/termination times.

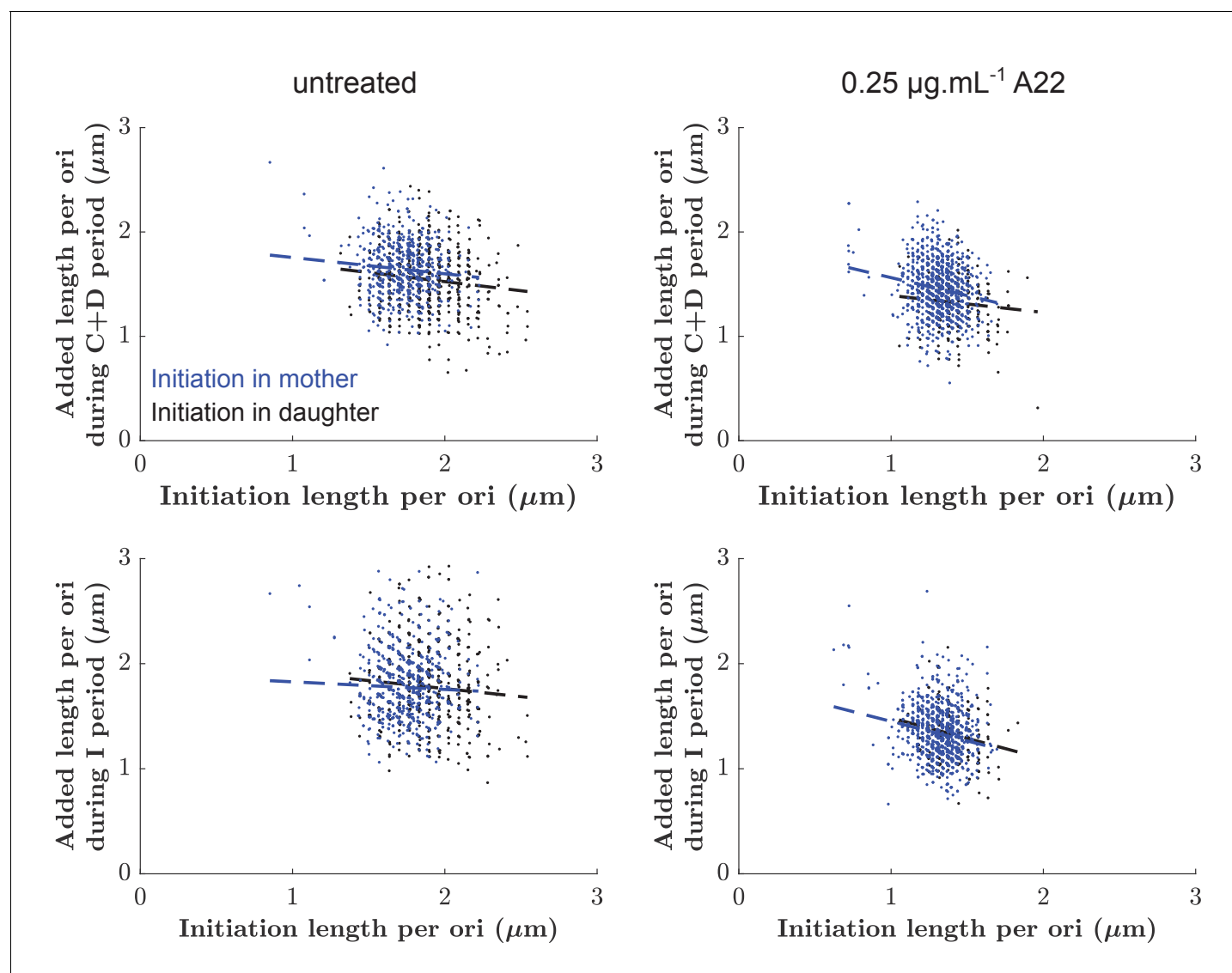


Figure 2—figure supplement 1. Detection of DNA replication in a single cell using the YPet-DnaN fusion. (A) Conditional probability density of the occurrence of YPet-DnaN foci as a function of cell length (y-axis) $p(y|t)dy$ as a function of time before subsequent cell division (x-axis) for untreated cells. Red and yellow squares represent the windows in which we are looking for initiation and termination respectively. (B, C) The DNA replication cycle can be detected based on the number of spots detected inside the cell, or, as chosen for this paper, based on the intensity distribution of the YPet-DnaN signal (see Materials and methods for details).

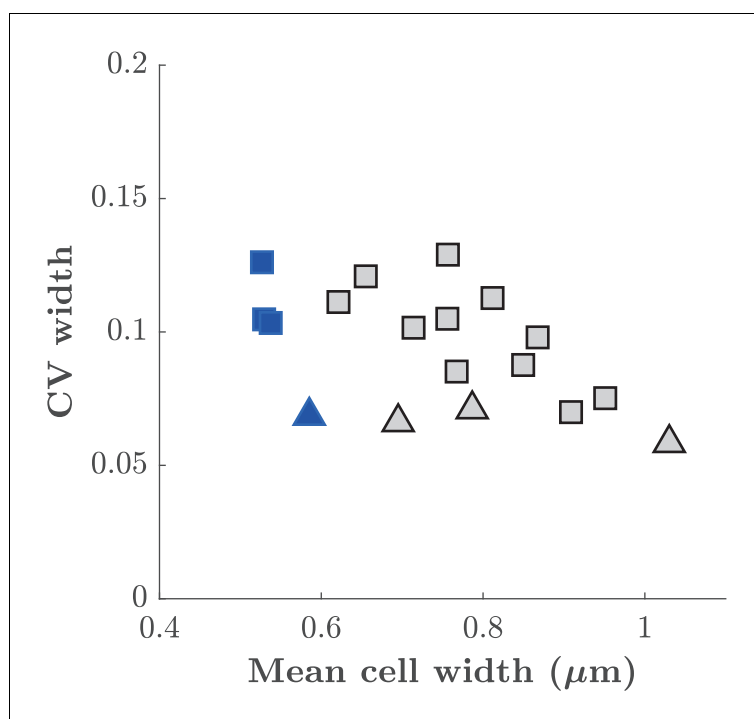


Figure 2—figure supplement 2. Cell-to-cell variation of cell width. Coefficient of variation of cell width as a function of mean cell width obtained at different A22 concentrations. Squares and triangles represent measurements performed on cells grown in mother machine or in liquid culture, respectively. Blue color represent wild-type cells. Gray color represent cells treated with different A22 concentrations.

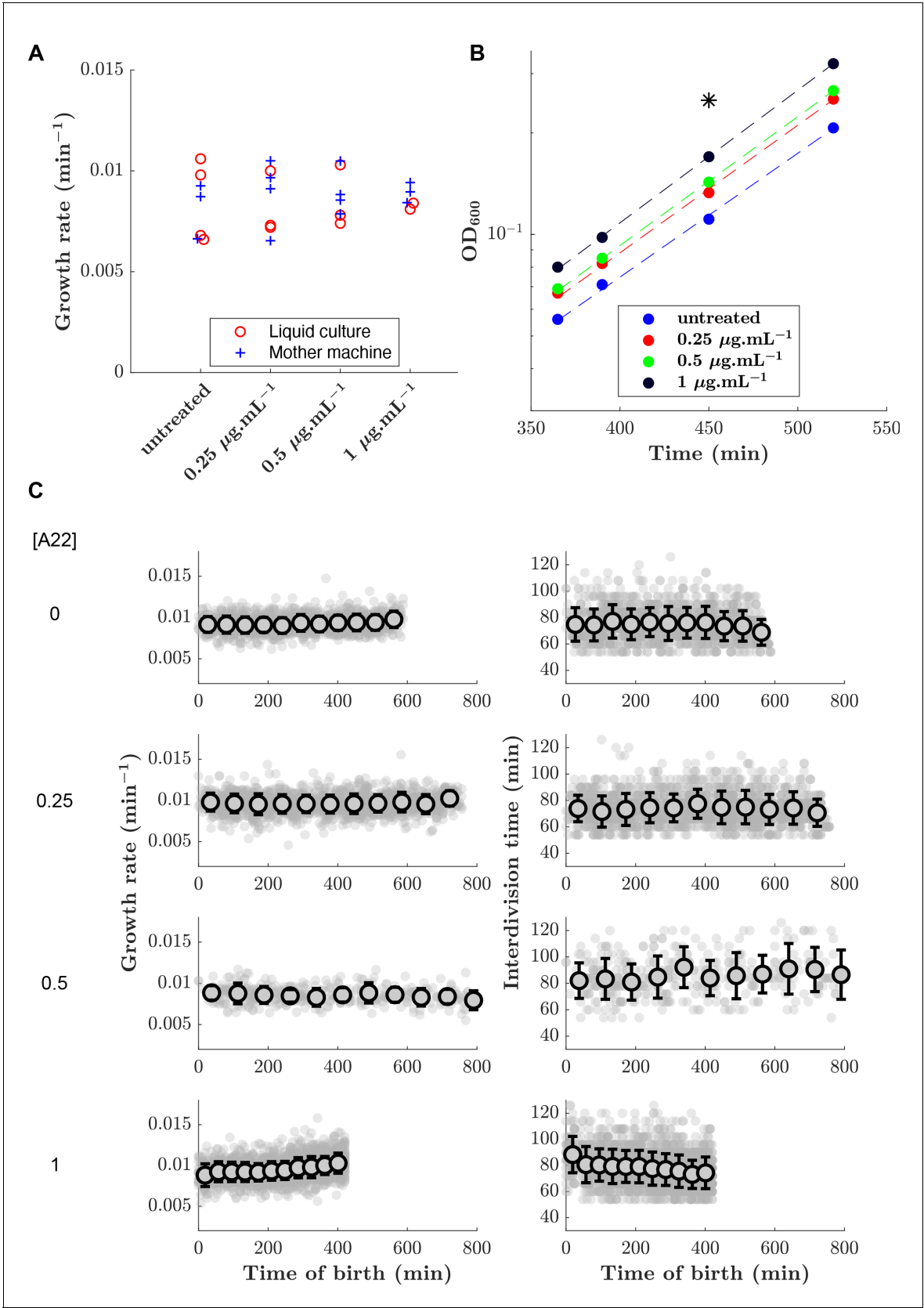


Figure 2—figure supplement 3. Growth rate and doubling time are maintained over time and upon A22 treatment. (A) Effect of A22 treatment on growth rate measured in liquid culture and in mother machine. (B) Example of growth curves obtained in liquid culture. The star indicates the time at Figure 2—figure supplement 3 continued on next page

Figure 2—figure supplement 3 continued

which the snapshots (**Figure 2A**) were taken. Dashed lines represent exponential fits. (**C**) Growth rate (left column) and doubling time (right column) remains approximately constant over time in the mother-machine experiments upon treatment with different A22 concentrations (with <15% variations during the observation window).

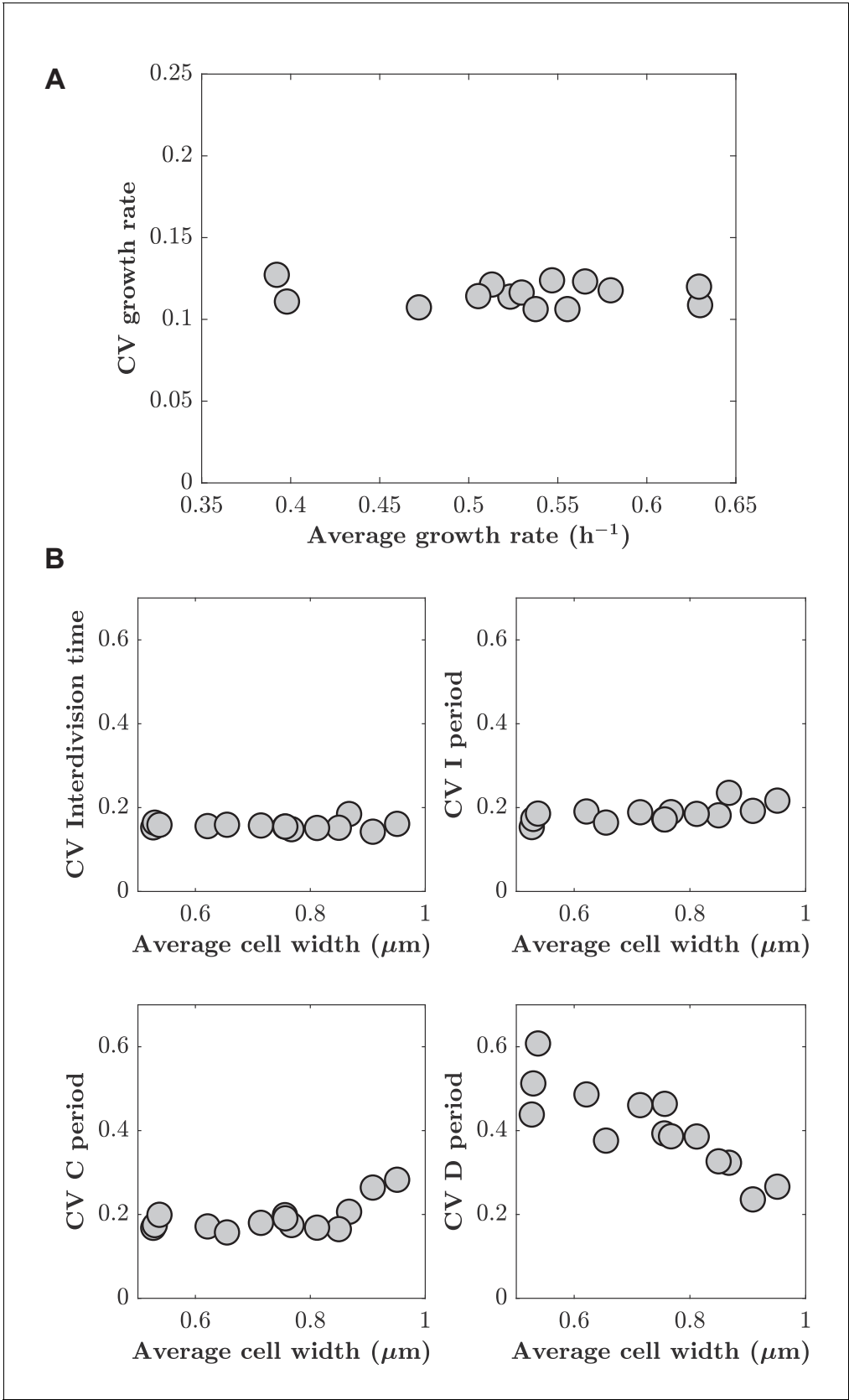


Figure 2—figure supplement 4. Cell-to-cell variations of different cell-cycle periods are independent of A22 treatment. (A) Coefficient of variation of growth rate as a function of average growth rate. (B) Cell-to-cell variations (coefficient of variation) of inter-division time, I, C, and D period do not increase with increasing average cell width. Each point represents one biological replicate generated in mother machine.

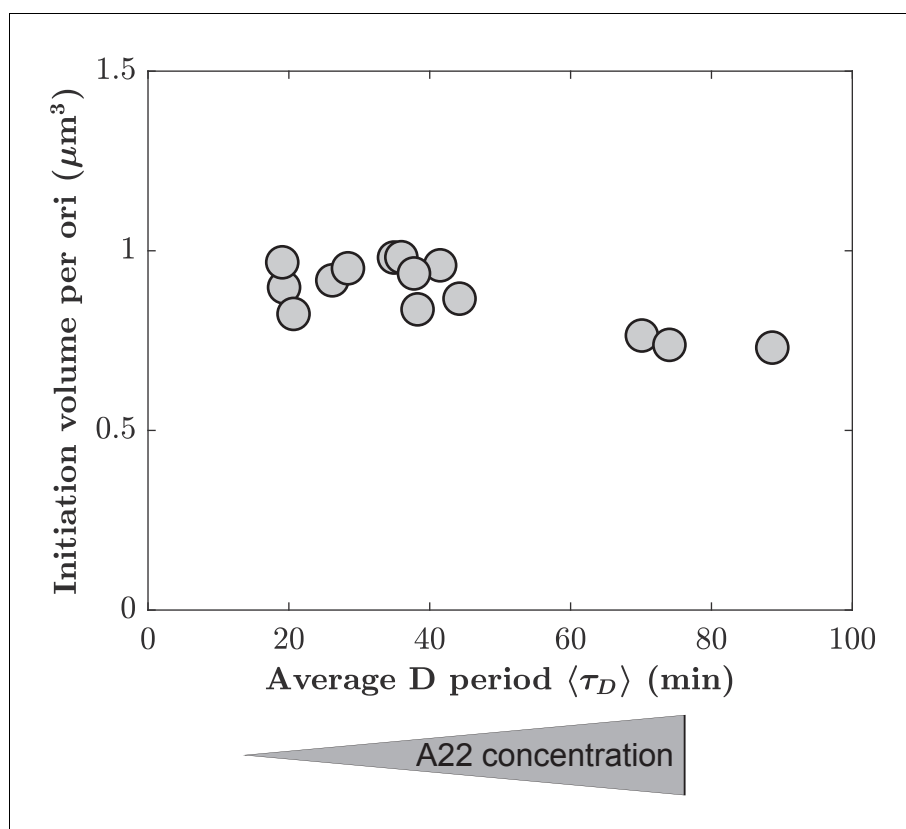


Figure 2—figure supplement 5. Mean initiation volume per ori as a function of average D period. Mean initiation volume is computed from individual lengths and mean width at the time of replication initiation, assuming spherocylindrical cells.

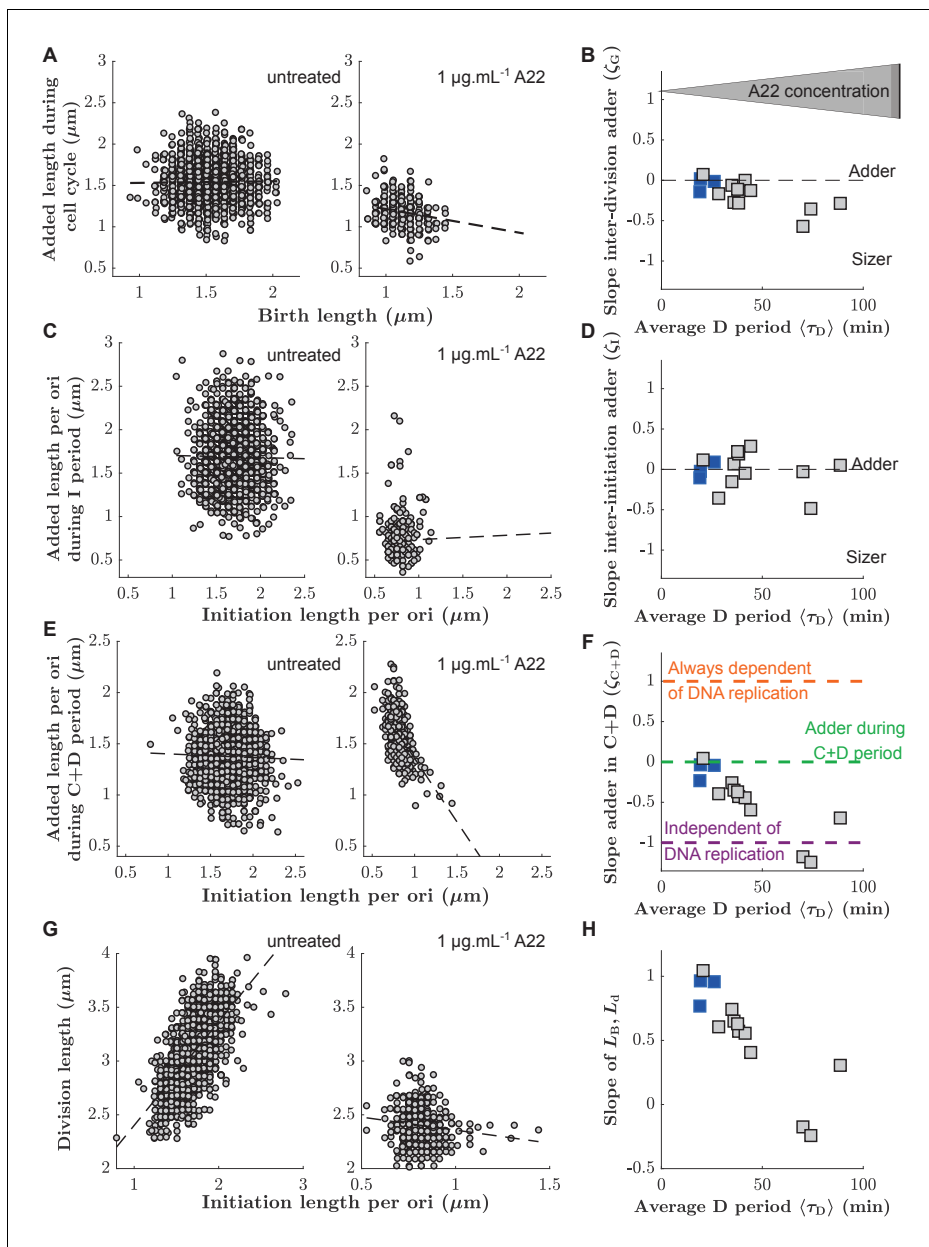


Figure 3. Single-cell correlations between division and DNA replication events. (A,C,E) Added size between birth and division (A), between subsequent events of replication initiation (C), and during the C+D period (E), for untreated cells (left) and cells treated with $1 \mu\text{g.mL}^{-1}$ A22 (right). Points represent single cells. Dashed lines represent robust linear fits. All lengths are indicated in units of μm . (B,D,F) Slopes of the added sizes corresponding to A, C, E, respectively, as a function of the D period as obtained through sub-lethal A22 treatment ($0-1 \mu\text{g.mL}^{-1}$). A slope of 0 represents adder behavior, while a slope of -1 represents independence on the size at the beginning of the sub-period (sizer behavior). Blue and gray squares represent unperturbed conditions and A22-treatment, respectively. Each symbol represents an independent biological replicate. (G,H) Division size L_d as a function of initiation size per ori L_B/n_{ori} (G) and corresponding slopes (H) in analogy to panels A, B, respectively. The decreasing slope in H demonstrates decreasing dependency of division on DNA replication.

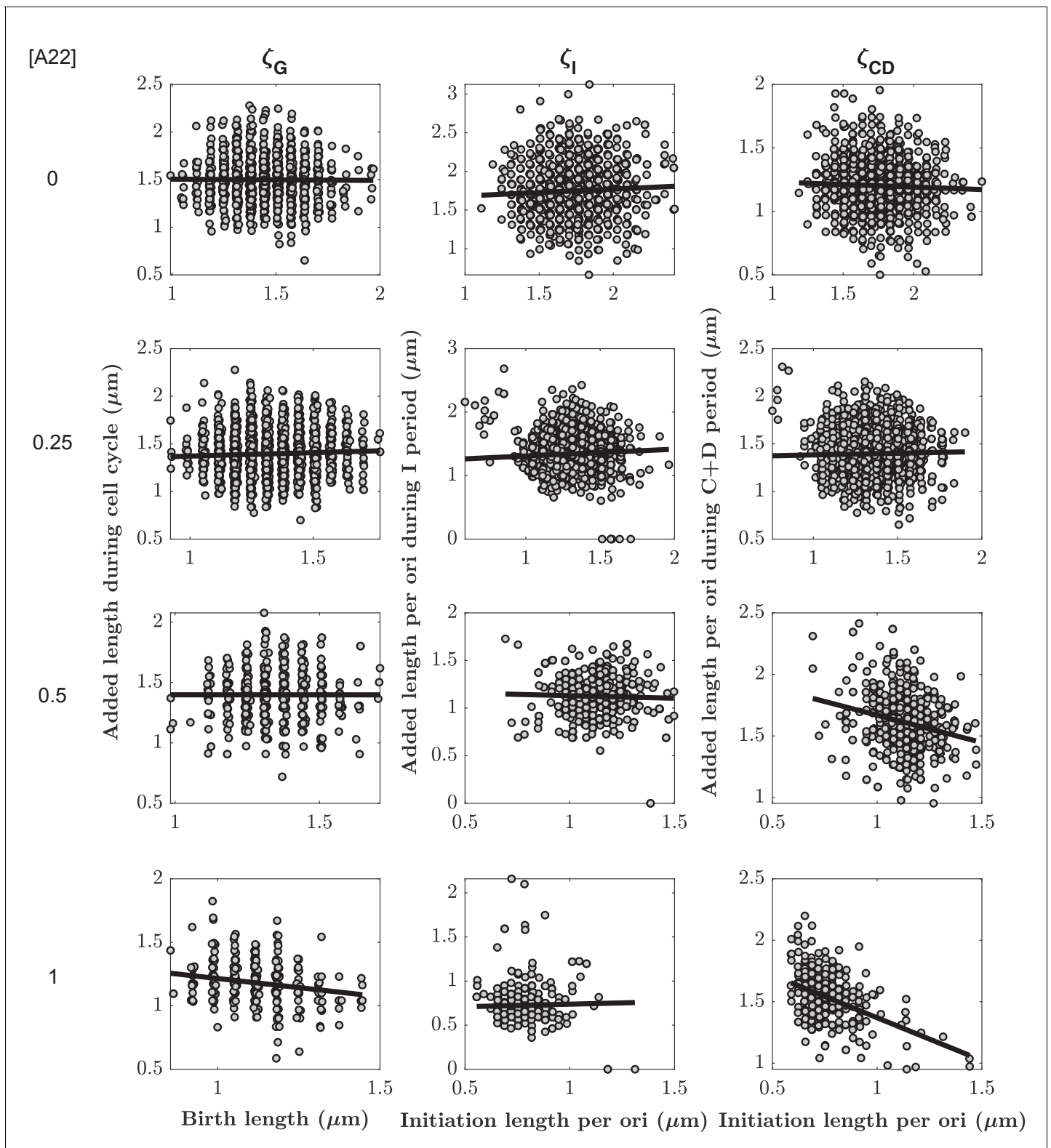


Figure 3—figure supplement 1. Added lengths during different subperiods as a function of the size at the beginning of the respective subperiod for different A22 concentrations. The slopes ζ_G , ζ_I , and ζ_{CD} for different A22 concentrations are obtained from robust fits (black lines). Each cloud represents one of three biological replicates.

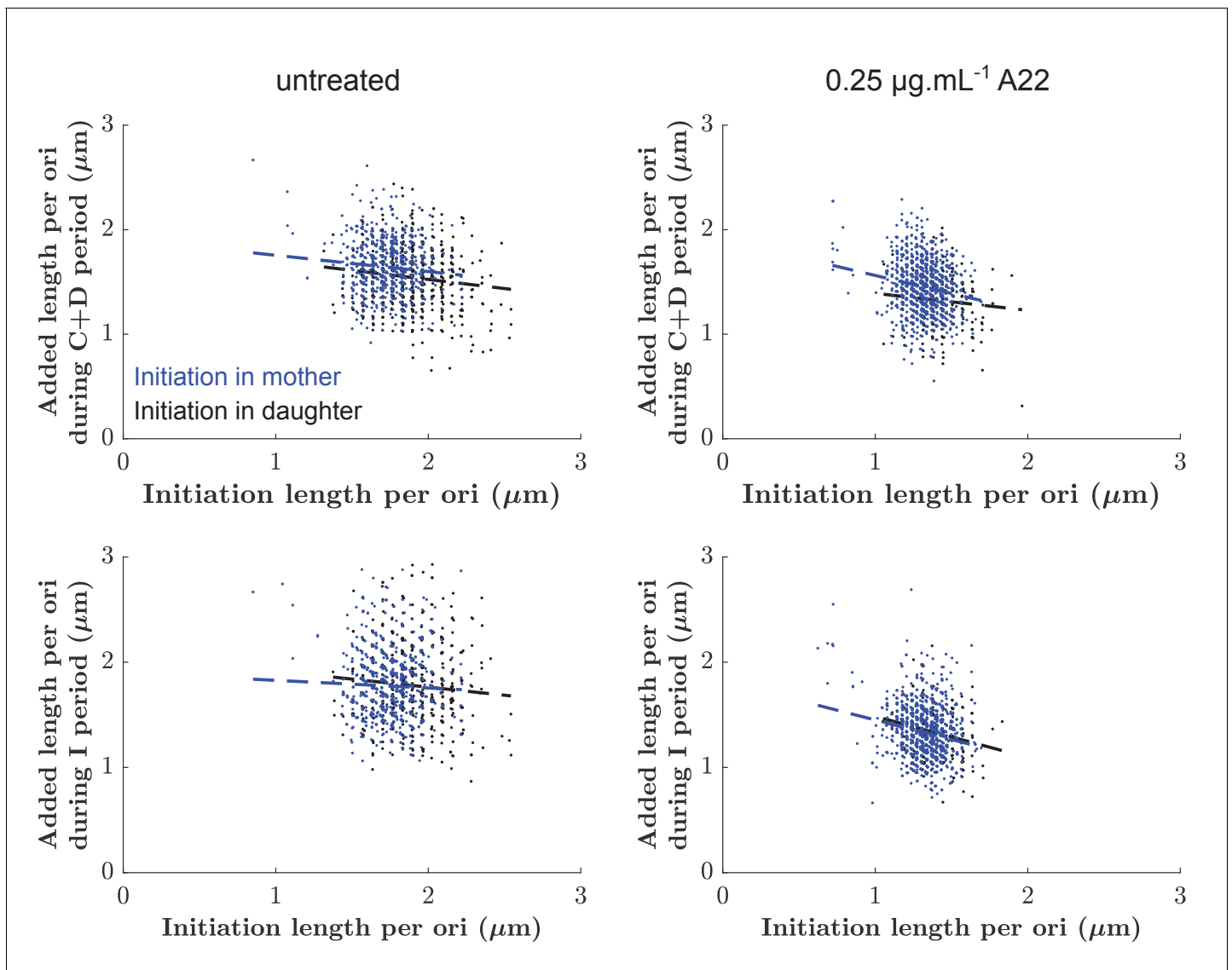


Figure 3—figure supplement 2. Added lengths during C+D period (top) or I period (bottom) as a function of the size at initiation for untreated cells (left) and cells treated with 0.25 $\mu\text{g/ml}$ A22 (right). Points are color-coded according to whether initiation happened in the mother (blue) or in the mother (black), respectively. Dashed lines represent the slopes of each cloud according to linear regression.

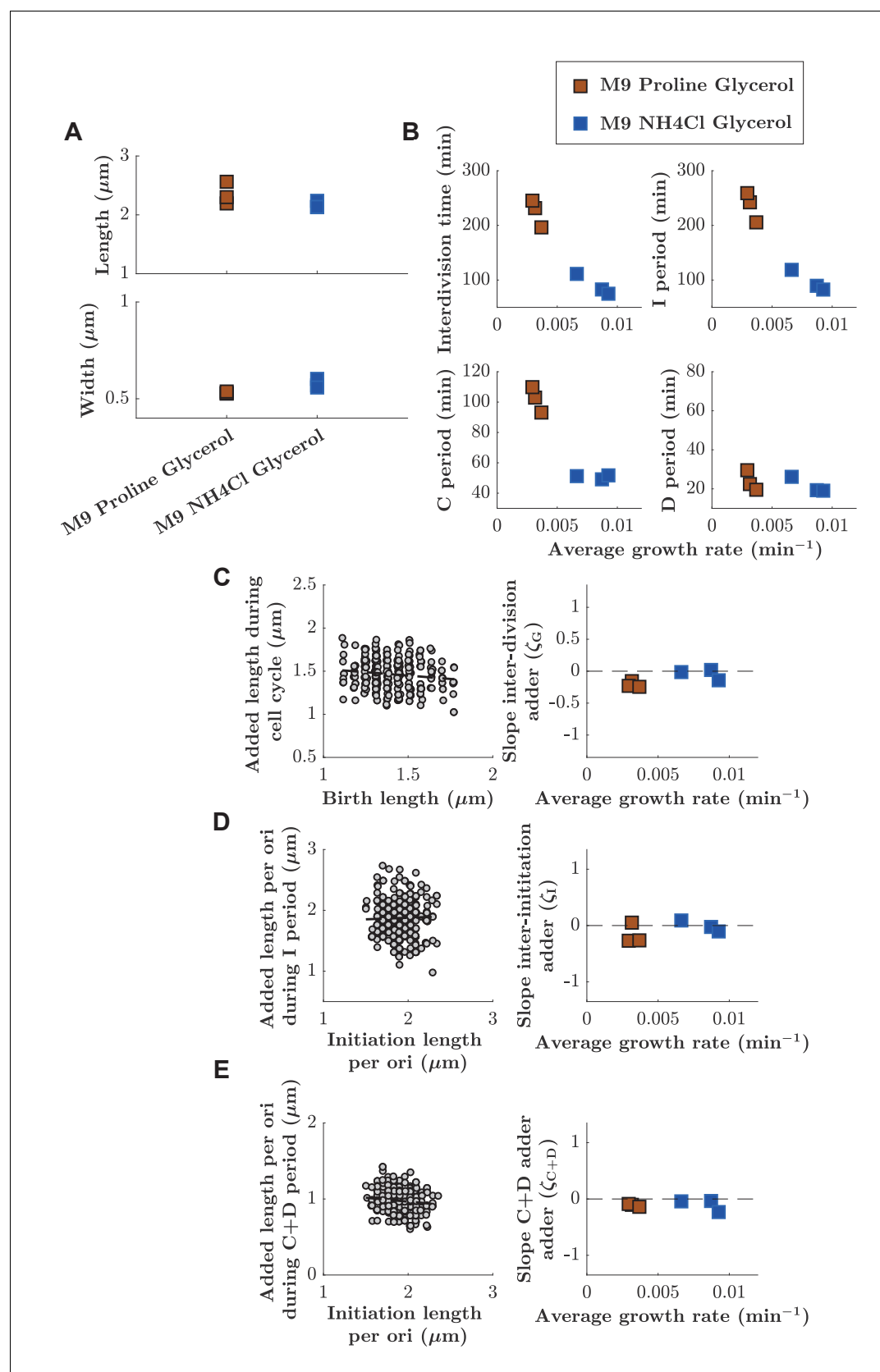


Figure 3—figure supplement 3. Adder behaviors for cell cycle, I period, and C+D period are robustly maintained at two different growth rates. (A) Lengths and widths obtained for cells grown in two different growth media: M9 Glycerol NH4Cl (blue squares) or M9 Glycerol Proline (red squares). Figure 3—figure supplement 3 continued on next page

Figure 3—figure supplement 3 continued

Symbols represent independent biological replicates. **(B)** Duration of inter-division time, I period, C period, and D period as a function of average growth rate measured in mother machines. **(C, D, E)** Left: Example of division, inter-initiation and C+D adder plots for cells grown at slower growth rate (M9 Proline Glycerol). Right: Slope of division, inter-initiation and C+D adder as a function of average growth rate for cells grown in the two different growth media (M9 Proline Glycerol and M9 NH₄Cl Glycerol).

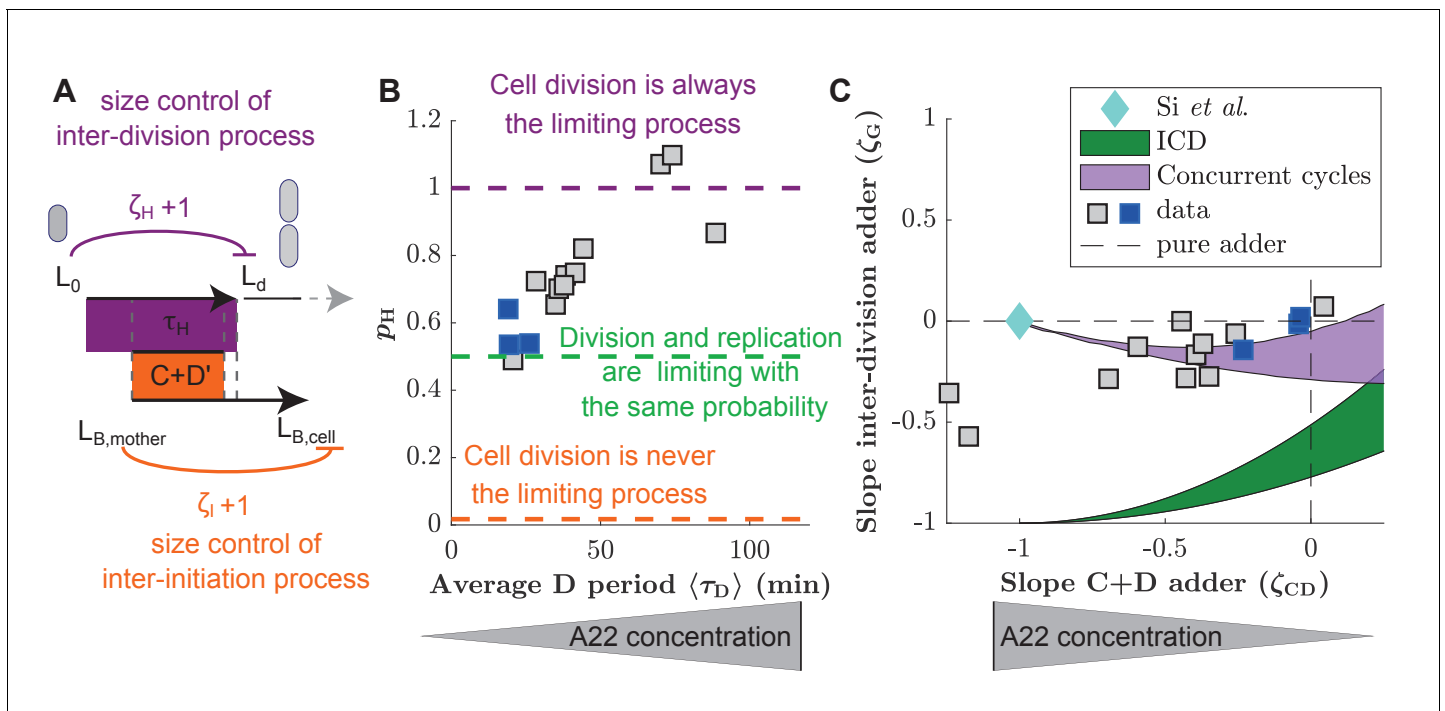


Figure 4. Experimental validation of the concurrent cycles model. **(A)** Cartoon: Two independent inter-division and timer-like replication/segregation must be completed before division occurs. The inter-division process is assumed to exhibit adder-like behavior with control parameter $\zeta_H = 0$, while the replication/segregation is a timer (see Materials and methods for details on the estimation). The adder-like inter-initiation processes with control parameter $\zeta_I = 0$ determines size at initiation. **(B)** Model-fitting to experimental data reveals the probability p_H of the inter-division process to control cell division as a function of increasing D period (with increasing A22 concentration), assuming constant control parameters $\zeta_H = 0$ and $\zeta_I = 0$. **(C)** Slopes of adder plots ζ_G as a function ζ_{CD} . Blue diamond: prediction in *Si et al., 2019*. Dotted lines: Prediction of pure adder models. Green: Prediction from a general class of single-process chromosome-limited models ('ICD' models, see Supplementary Notes) (*Micali et al., 2018b*), where cells divide after completion of the replication/segregation process with variable ζ_{CD} . Purple: Prediction of the concurrent cycles model. Shaded areas represent the ranges of predictions using the maximum and minimum experimentally measured input parameters (ratio of variance of size at initiation over size at birth; ratio of mean size at division over size at birth). **(B, C)** Blue and gray squares represent unperturbed conditions and A22-treatment, respectively. Each symbol represents an independent biological replicate.

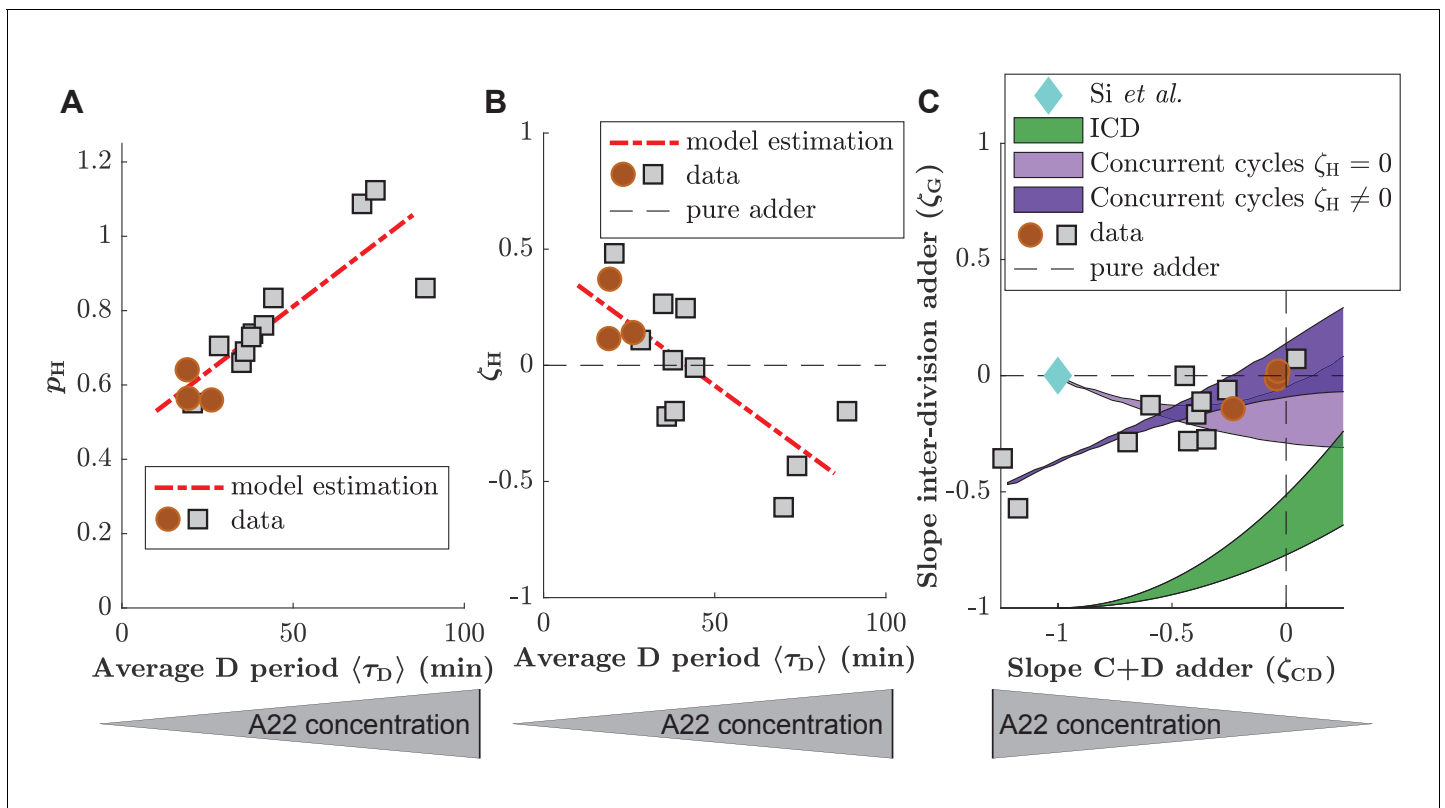


Figure 4—figure supplement 1. Predictions of the concurrent cycles model if ζ_H is left as a free parameter. (A, B) Probability for the cell division process to be limiting (p_H) (A) and strength of the inter-division control parameter (ζ_H) (B) for experimental data generated in this study (red circles and grey squares for untreated cells and cells treated with A22). Both p_H and ζ_H are allowed to vary and the values are estimated solving Equation (S20) for p_H and ζ_H . The linear fit for the different results is shown as red dashed line. (C) ζ_G (division adder slope) as a function of ζ_{CD} (C+D adder slope) for data generated in this study (gray circles). Prediction of the replication-independent model by Si et al., 2019 (blue diamond), and of ICD model (green area). Two predictions of the concurrent cycles model are also plotted: light purple: prediction of concurrent cycles model assuming $\zeta_H = 0$ (see Figure 4). Dark purple: prediction of concurrent cycles model leaving ζ_H as a free parameter of the fit (see (A,B)). The shaded areas represent the range of predictions using the maximum and minimum of experimentally measured ratio of variance of size at initiation over size at birth (both for ICD and concurrent cycles) and of the experimentally measured ratio of mean size at division over size at birth (concurrent cycles). The maximum and minimum values are taken over the experimental data reported in this picture, that is treated and untreated data acquired for this work.

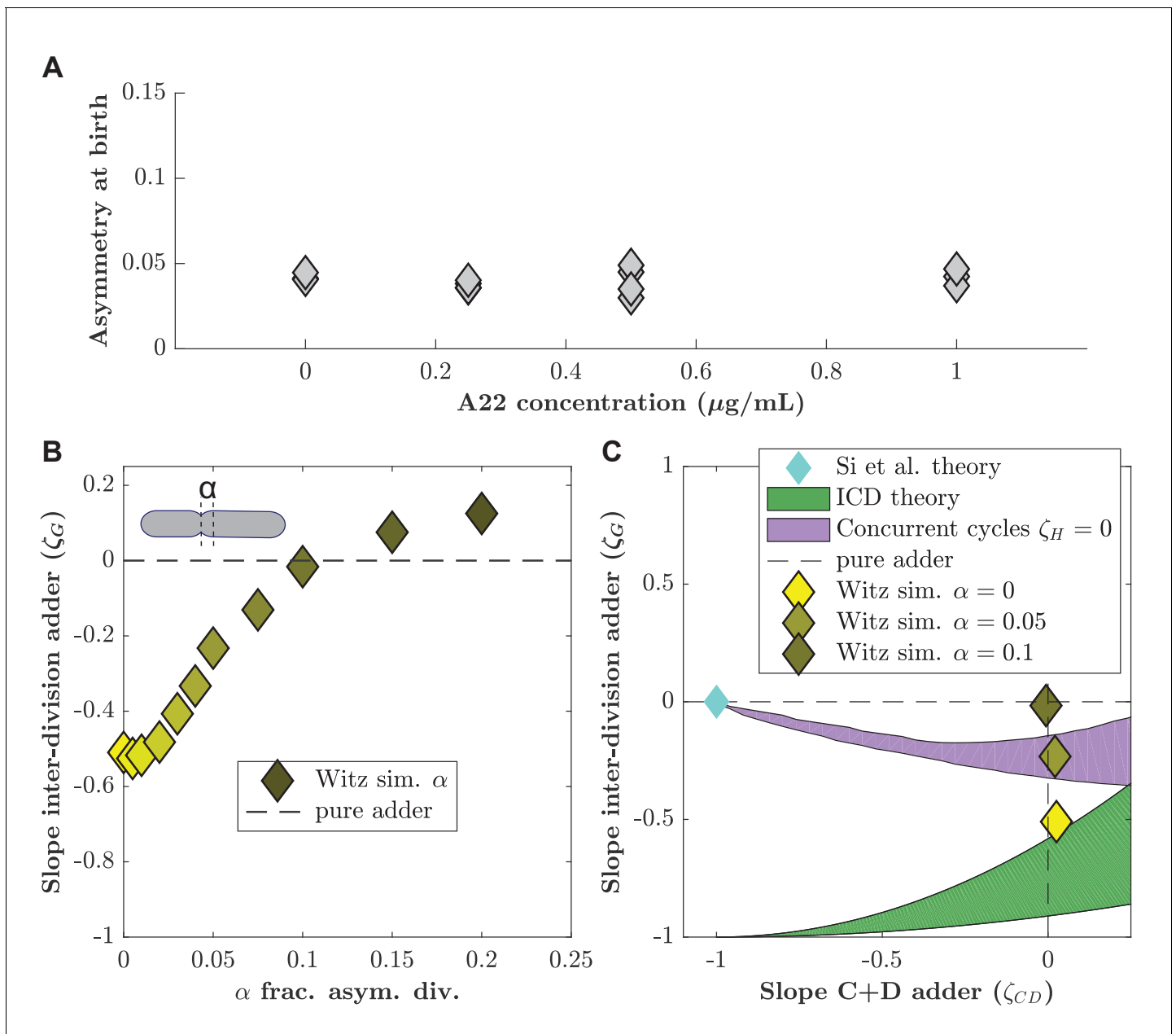


Figure 4—figure supplement 2. Asymmetric division drives C+D to adder behavior in ICD single-process models. Witz and coworkers (Witz et al., 2019) proposed an ICD model (see methods) with an adder between consecutive initiations ($\zeta_I = 0$) and in the C+D period ($\zeta_{CD} = 0$), and asymmetric division, which we tested with our data. (A) The level of asymmetry at birth from our data is about 5%. The asymmetry is computed as $\frac{(L_0^{cell1} - L_0^{cell2})}{(L_0^{cell1} + L_0^{cell2})}$ (where cell 1 and cell 2 are two daughter cells) and averaged for each dataset. (B) Simulations of the Witz et al. 'double adder' ICD model as a function of the asymmetry in division (α). (Parameter set as in untreated conditions: $\langle \mu \rangle = 0.0088 \text{ min}^{-1}$, $\sigma_\mu = 0.001 \text{ min}^{-1}$, $\langle \Delta_I \rangle = 0.875 \text{ } \mu\text{m}^3$, $\sigma_{\Delta_I} = 0.19 \text{ } \mu\text{m}^3$, $\langle \Delta_{CD} \rangle = 1.39 \text{ } \mu\text{m}^3$, $\sigma_{\Delta_{CD}} = 0.16 \text{ } \mu\text{m}^3$). For increasing asymmetry, the model recapitulates the near-adder behavior between divisions ($\zeta_G \approx 0$). (C) ζ_G (division adder slope) as a function of the C+D adder slope ζ_{CD} for simulations at $\alpha = 0$ (bright yellow diamond), $\alpha = 0.05$ (bright yellow), and $\alpha = 0.1$ (dark yellow diamond). In our own experimental study find the division asymmetry to be about 5% ($\alpha = 0.05$), consistent with previous reports. Blue diamond: prediction from the Si et al. model. Green shaded area: Prediction of the ICD model with no asymmetry in division. Purple shaded area: Prediction of the concurrent cycles model with the hypothesis that $\zeta_H = 0$. The shaded areas represent the range of predictions using the maximum and minimum experimentally measured ratio of variance of size at initiation over size at birth (both for ICD and concurrent cycles models) and the experimentally measured ratio of mean size at division over size at birth (for the concurrent cycles model). The maximum and minimum values are taken over the untreated conditions acquired for this work as well as the published data from Si et al., 2019 and Witz et al., 2019.

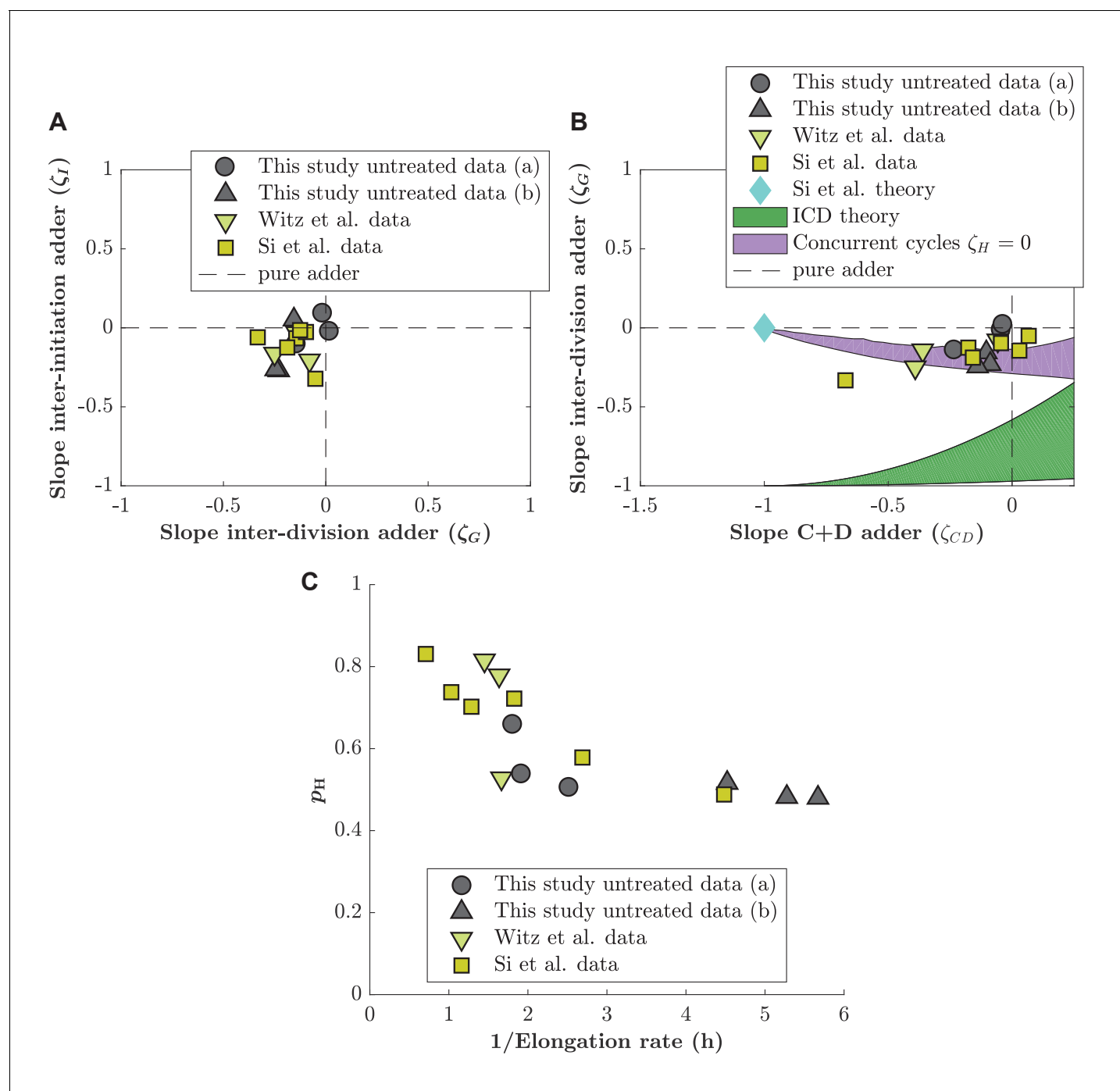


Figure 4—figure supplement 3. Comparison of adder slopes for data of unperturbed cells generated by different labs. **(A)** Inter-division adder slope (ζ_G) plotted as a function of inter-initiation slope (ζ_I). Gray circles: data generated in M9(NH₄Cl) Glycerol medium. Gray triangles: data generated in M9 (Proline) Glycerol medium (slow growth rate). Green triangle: data generated by *Witz et al., 2019*. Yellow square: data generated by *Si et al., 2019*. **(B)** Division adder slope (ζ_G) as a function of the C+D adder slope (ζ_{CD}). Same symbols as in **(A)** correspond to the same data. Additionally, we also display predictions from different models as in **Figure 4—figure supplement 2**. **(C)** Estimation of p_H as a function of doubling time for data generated in this study, *Witz et al., 2019* and *Si et al., 2019*.

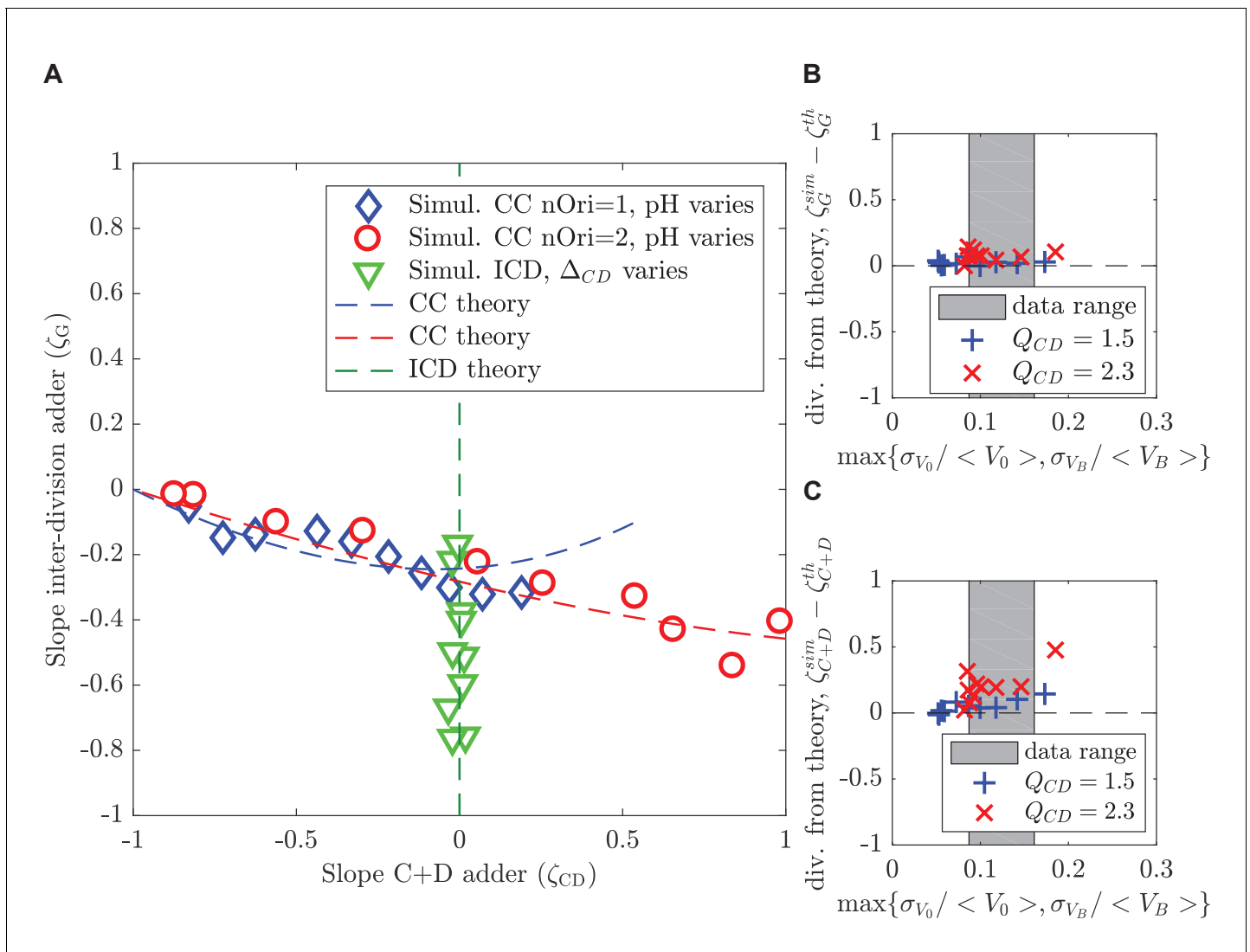


Figure 4—figure supplement 4. Theoretical predictions in the small-noise approximations agree with simulations at realistic noise levels. **(A)** The plot shows the slope of the inter-division adder plot ζ_G as a function of the slope of the adder plot in the $C + D$ period ζ_{CD} for both the concurrent cycles model (blue and red) and for the ICD model (green), respectively. Theoretical predictions in the small-noise approximation (dashed lines) agree with simulations (symbols). For concurrent cycles, simulation parameters are chosen to maintain noise levels comparable to untreated experimental conditions and to remain on average in the regime of no overlapping rounds (blue diamonds) or a single overlapping round (red circles), while varying p_H . For ICD (green triangles), Δ_{CD} varies in conditions without overlapping rounds. The ratio $\langle \tau_{C+D} \rangle / \langle \tau \rangle$ ranges from 0.5 to 1.5. **(B, C)** The analytical predictions are robust with increasing noise levels. The plots show the difference between the analytical (small-noise) predictions and direct simulations of the size homeostasis parameter ζ (slope of the adder plot) for the inter-division cycle **(B)** and for the $C + D$ period **(C)** in the concurrent cycles model, as a function of the maximal relative noise level. Simulation parameters are set to explore the limits of the small noise approximation while maintaining constant p_H and Q_{CD} . The gray region indicates the regime of noise levels obtained from our experiments. The $Q_{CD} = 1.5$ regime correspond to $\langle \tau_{C+D} \rangle / \langle \tau \rangle \approx 0.6$ (blue + crosses), $Q_{CD} = 2.3$ regime correspond to $\langle \tau_{C+D} \rangle / \langle \tau \rangle \approx 1.2$ (red x crosses).

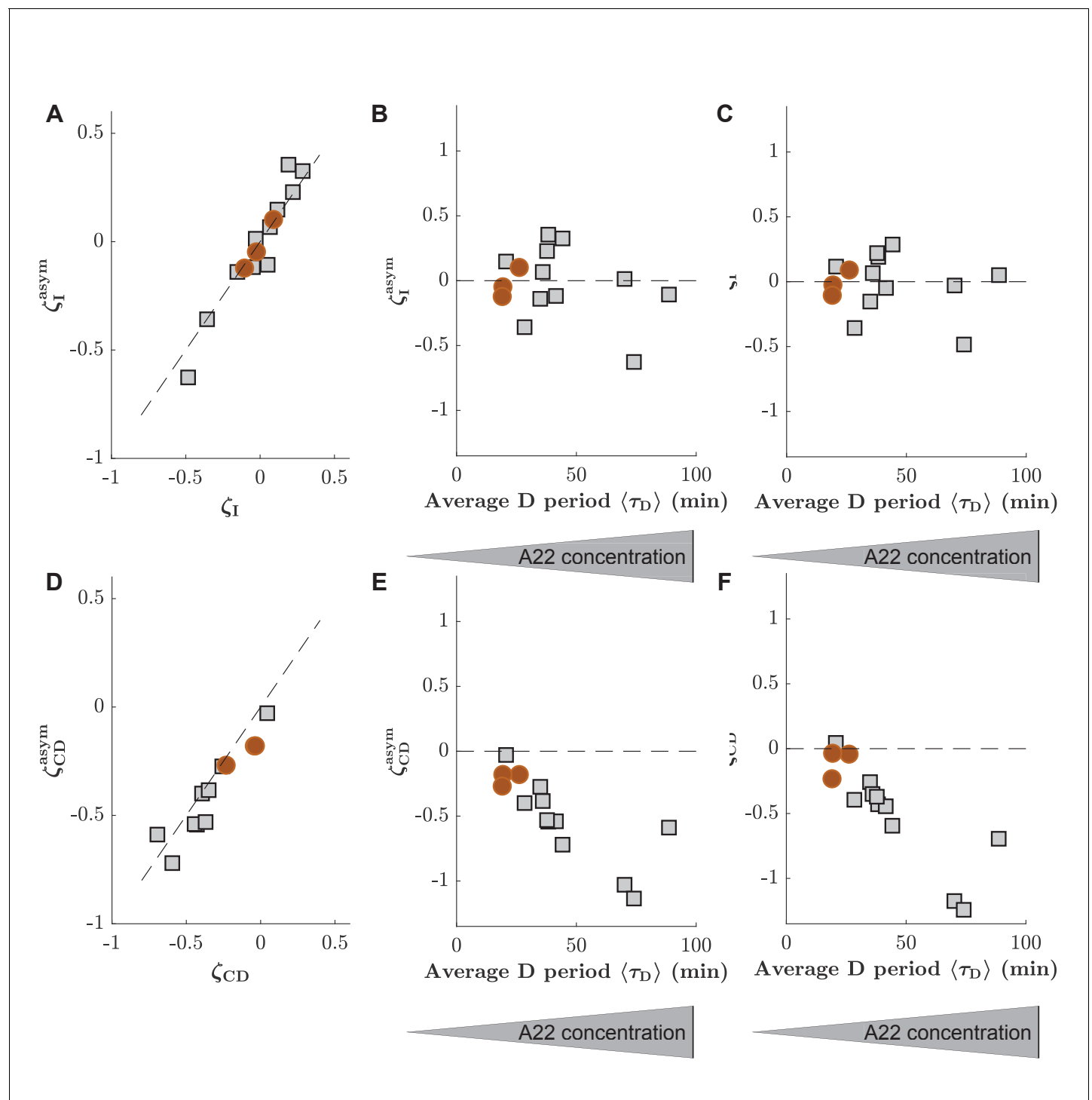


Figure 4—figure supplement 5. The consideration of asymmetry of cell division has no significant effect on slopes of inter-initiation adder and adder during C+D period. (A) Comparison of inter-initiation adder slope (ζ_I) calculated in two different ways, either by assuming symmetric cell division (y-axis, obtained from $L_B^{cell}/n_{cell} - L_B^{mother}/n_{mother}$, where n_x is the number of origins at the time of replication initiation in the mother or cell), or by taking asymmetry into account (x-axis, obtained through correction as indicated in Materials and methods). (B) ζ_I as a function of the average D period, assuming symmetric division. (C) ζ_I^{asym} as a function of the average D period, correcting for asymmetric division. (D-E) Comparison of the adder slopes during the C+D period generated while ignoring or considering division asymmetry. Panels are analogous to panels (A–C). Circles (red) and squares (gray) represent unperturbed conditions and A22-treatment, respectively. Each symbol represents an independent biological replicate.